Global Scientific JOURNALS

GSJ: Volume 8, Issue 9, September 2020, Online: ISSN 2320-9186
www.globalscientificjournal.com

Control of quadrotor by designing Third-order Supertwisting SMC

Mebaye Belete Mamo[1]
[1]*Addis Ababa Science and technology university, Ethiopia*
Mebaye.belete@aastu.edu.et

Abstract— This paper studies the modeling and control of quadcopter. It models the quadcopter nonlinear dynamics using Lagrange formalism and design controller for attitude (pitch & roll), heading & altitude regulation of quadrotor. Mathematical modeling includes aerodynamic effects and gyroscopic moments. One Non-linear Control strategy, Third-Order SMC based on a super-twisting algorithm has been proposed. Third-Order SMC Controller is designed for regulation control problem with the four control variables. The Controller has been implemented on the quadrotor physical model using Matlab/Simulink software. Finally, the performance of the proposed controller was demonstrated in the simulation study. The simulation results show excellent modeling and control performance.

Index Terms— HOSMC, Lagrange, Mathematical Modelling, Quadrotor, MATLAB/Simulink.

1. INTRODUCTION

An Unmanned Aerial Vehicle (UAV) refers to a flying machine without an on-board human pilot [1], [2]. These vehicles are being increasingly used in many civil domains, especially for surveillance, environmental researches, security, rescue, and traffic monitoring.

Under the category of rotorcraft UAVs, Quadrotor has acquired much attention among researchers. The quadrotor is a multi-copter that is lifted and propelled by four rotors, each mounted on one end of a cross-like structure. Each rotor consists of a propeller fitted to a separately powered Brushless DC motor. The quadcopter has six degrees of freedom (three translational and three rotational) and only four actuators [3]. Hence, the quadcopter is an underactuated, highly nonlinear, and coupled system.

Several linear control approaches, such as PID, Linear Quadratic Regulator (LQR), and Linear Quadratic Gaussian(LQG), have been proposed in the literature and applied for attitude stabilization and/or altitude tracking of Quadrotors[13], [14]. However, these methods can impose limitations on the application of quadrotors for extended flight

Regions, i.e., aggressive maneuvers, where the system is no longer linear.

Moreover, the stability of the closed-loop system can only be achieved for small regions around the equilibrium point, which are extremely hard to compute. Besides, the performances of these control laws on attitude stabilization are not satisfactory enough compared with other more advanced methods.

To overcome this problem, nonlinear control alternatives, such as feedback linearization, SMC [15], [16], [17], and Backstepping [18] approaches are recently used in the VTOL aircraft control framework. An integral predictive nonlinear H∞ strategy has been also proposed and applied by G.V. Raffo et al. in [19].

In summary, the literature on quadrotor control ignores the aerodynamic effects, air disturbance, and gyroscopic moments in the dynamic modeling of the quadrotor. Besides, in the case of sliding mode controller implementation, it does not reduce both the control effort and the chattering effect.

This paper uses a novel approach to address the above problems. It also designed a novel Third-order SMC controller with minimum tracking error.

The paper is organized into five sections. In section 1, it introduces quadrotor UAV. In Section 2, it models the physical system by considering the aerodynamic and gyroscopic effects. In Section 3, it designs second-order SMC based on the supertwisting algorithm. In Section 4, present the simulation results obtained from the control implementation of the physical system in the Simulink environment. Finally, in Section 5, it shows the control inputs and then concludes the work.

2. MATHEMATICAL MODELLING

In this section, a complete dynamical model of the Quadrotor UAV is established using the Lagrange formalism.

2.1 Rotational Matrix

The orientation of the quadrotor is represented by Euler angles (pitch, roll, and yaw).To transform the body-fixed frame into the inertial frame; the z-y-x rotational matrix is considered [4].

To avoid the system singularities, it is important to assume the angle bound

$$\frac{-\pi}{2}<\varphi<\frac{\pi}{2};\frac{-\pi}{2}<\theta<\frac{\pi}{2};-\pi<\psi<\pi \quad (2.1)$$

$$R_{(x,\varphi)}=\begin{pmatrix}1 & 0 & 0\\ 0 & c\varphi & -s\varphi\\ 0 & s\varphi & c\varphi\end{pmatrix} \quad R_{(y,\theta)}=\begin{pmatrix}c\theta & 0 & s\theta\\ 0 & 1 & 0\\ -s\theta & 0 & c\theta\end{pmatrix}$$

$$R_{(z,\psi)}=\begin{pmatrix}c\psi & -s\psi & 0\\ s\psi & c\psi & 0\\ 0 & 0 & 1\end{pmatrix} \quad (2.2)$$

The Euler rotation about z-y-x or R_{xyz} is given by

$$R_{xyz}=R_{(z,\psi)}\,R_{(y,\theta)}\,R_{(x,\varphi)}$$

$$=\begin{pmatrix}c\psi c\theta & s\varphi s\theta c\psi-s\psi c\varphi & c\varphi s\theta c\psi+s\psi s\varphi\\ s\psi c\theta & s\varphi s\theta s\psi+c\psi c\varphi & c\varphi s\theta s\psi-s\varphi c\psi\\ -s\theta & s\varphi c\theta & c\varphi c\theta\end{pmatrix} \quad (2.3)$$

The studied Quadrotor rotorcraft is detailed with their body- and inertial frames $F_b=(b,x^b,y^b,z^b)$ and $F_i=(G,x^G,y^G,z^G)$ respectively.

The model partitions naturally into translational and rotational coordinates [6]

$$\xi=(x,y,z)\in\mathbb{R}^3 \qquad \eta=(\varphi,\theta,\psi)\in\mathbb{R}^3 \quad (2.4)$$

$\xi=(x,y,z)$ denotes the position vector of the center of mass of the Quadrotor relative to the fixed inertial frame and $\eta=(\varphi,\theta,\psi)$ denotes the orientation of quadrotor to the inertial frame. This is shown in Figure 1 below

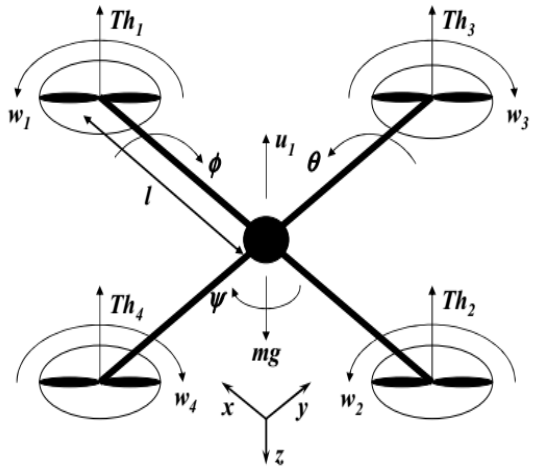

Figure 1 Typical quadrotor schematic diagram with the body and inertial frames [5]

1.2 Forces, Moments, and Torques on Quadrotor

2.2.1 Thrust forces

The quadrotor has four propellers so that it produces four thrust forces.

$$\mathbf{F}=\sum_{i=1}^{4}\mathbf{F}_i \quad (2.5)$$

$$F=F_1+F_2+F_3+F_4 \quad (2.6)$$

2.2.2 Moments

Gyroscopic Moment: There are two gyroscopic torques, this is due to the motion of the propellers (Mgp) and the quadrotor body (Mgb) [11] given by:

$$M_{gp}=\sum_{i=1}^{4}\Omega\wedge\left[0,0,J_r(-1)^{i+1}w_i\right]^{\mathrm{T}} \quad (2.7)$$

$$M_{gb}=\Omega\wedge J\Omega \quad (2.8)$$

$$J=\begin{pmatrix}I_{xx} & 0 & 0\\ 0 & I_{yy} & 0\\ 0 & 0 & I_{zz}\end{pmatrix} \quad (2.9)$$

Since the quadrotor geometry is symmetric, Ixy = Ixz= Iyx = Iyz = Izx = Izy = 0.Where Ω is the vector of angular velocity in a fixed earth frame.

$$\Omega=\begin{pmatrix}\dot{\varphi}\\ \dot{\theta}\\ \dot{\psi}\end{pmatrix}$$

Aerodynamic friction moment: the quadrotor moves in the air, due to this it is subjected to aerodynamic friction. The torque caused by this aerodynamic friction is called the aerodynamic friction moment. It is given by:

$$M_a=diag(k_4,k_5,k_6)\begin{pmatrix}\dot{\varphi}^2 & \dot{\theta}^2 & \dot{\psi}^2\end{pmatrix}^T \quad (2.10)$$

$diag(k_4,k_5,k_6)$ are aerodynamic friction coefficient and $\dot{\eta}^2$ are angular velocity square vector for rotational dynamics.

2.2.3 Torques

Pitch torque

It is directly proportional to the difference of thrust force generated by the second and fourth propellers $(F_4\text{-}F_2)$ [7-9].

$$\tau_\varphi = l(F_4 - F_2) \tag{2.11}$$

Roll torque

It is directly proportional to the difference of thrust force generated by the first and Third propellers $(F_3\text{-}F_1)$ [7-9].

$$\tau_\theta = l(F_3 - F_1) \tag{2.12}$$

Yaw torque

which is directly proportional to the difference of thrust force generated by all the propellers [7-9].

$$\tau_\psi = c(F_1 - F_2 + F_3 - F_4) \tag{2.13}$$

1.3 Modeling with Lagrange formalism

To obtain the quadrotor dynamics in terms of Lagrange, we use the Lagrange partial differential equation.

$$\frac{d}{dt}\frac{\partial L}{\partial \dot{q}} - \frac{\partial L}{\partial q} = F \tag{2.14}$$

Where $F=\left(F_\xi, \tau\right)$. We can calculate the translational and rotational components as follows

$$\mathbf{R}_{xyz}\begin{pmatrix} 0 \\ 0 \\ \sum_{i=1}^{4} \mathbf{F}_i \end{pmatrix} - \begin{pmatrix} k_1 \dot{x} \\ k_2 \dot{y} \\ k_3 \dot{z} \end{pmatrix} = \mathbf{F}_\xi = \begin{pmatrix} (c\varphi s\theta c\psi + s\psi s\varphi)u_1 - k_1 \dot{x} \\ (c\varphi s\theta s\psi - s\theta c\psi)u_1 - k_2 \dot{y} \\ (c\varphi c\theta)u_1 - k_3 \dot{z} \end{pmatrix} \tag{2.15}$$

$$\begin{pmatrix} \tau_\varphi \\ \tau_\theta \\ \tau_\psi \end{pmatrix} - \mathbf{M}_a - \mathbf{M}_{gp} - \mathbf{M}_{gb} = \tau = \begin{pmatrix} \tau_\varphi - J_r \dot{\Omega}_r \dot{\theta} - (I_{zz} - I_{yy})\dot{\theta}\dot{\psi} - k_4 \dot{\varphi}^2 \\ \tau_\theta + J_r \dot{\Omega}_r \dot{\varphi} - (I_{xx} - I_{zz})\dot{\varphi}\dot{\psi} - k_5 \dot{\theta}^2 \\ \tau_\psi - (I_{yy} - I_{xx})\dot{\theta}\dot{\varphi} - k_6 \dot{\psi}^2 \end{pmatrix} \tag{2.16}$$

Computing the Lagrange partial differential equation for all the six generalized coordinates, we get the following differential equations

$$\ddot{x} = (c\varphi s\theta c\psi + s\psi s\varphi)\frac{u_1}{m} - \frac{k_1}{m}\dot{x} \tag{2.17}$$

$$\ddot{y} = (c\varphi s\theta s\psi - s\theta c\psi)\frac{u_1}{m} - \frac{k_2}{m}\dot{y} \tag{2.18}$$

$$\ddot{z} = (c\varphi c\theta)\frac{u_1}{m} - \frac{k_3}{m}\dot{z} - g \tag{2.19}$$

$$\ddot{\varphi} = \frac{\tau_\varphi}{I_{xx}} - \frac{J_r \dot{\Omega}_r}{I_{xx}}\dot{\theta} - \frac{(I_{zz} - I_{yy})}{I_{xx}}\dot{\theta}\dot{\psi} - \frac{k_4}{I_{xx}}\dot{\varphi}^2 \tag{2.20}$$

$$\ddot{\theta} = \frac{\tau_\theta}{I_{yy}} + \frac{J_r \dot{\Omega}_r \dot{\varphi}}{I_{yy}} - \frac{(I_{xx} - I_{zz})}{I_{yy}}\dot{\varphi}\dot{\psi} - \frac{k_5}{I_{yy}}\dot{\theta}^2 \tag{2.21}$$

$$\ddot{\psi} = \frac{\tau_\psi}{I_{zz}} - \frac{(I_{yy} - I_{xx})}{I_{zz}}\dot{\theta}\dot{\varphi} - \frac{k_6}{I_{zz}}\dot{\psi}^2 \tag{2.22}$$

3. CONTROL SYSTEM DESIGN

3.1 Third-order Sliding Mode Controller

3.1.1 Super-twisting algorithm

There are four major algorithms used for second-order sliding mode control design. These are Twisting, Sub-optimal, quasi-continuous, and Super-twisting.

All the first three algorithms need the measurements of sliding& sliding derivatives to guarantee the sliding and sliding derivatives to become zero. That is not the case in the Super-twisting algorithm, it only needs a measurement of the sliding surface to guarantee the two-sliding mode existence. For this reason, Super-twisting can be used instead of the conventional (first-order) sliding mode using the same available information. Besides, it reduces chattering to a higher extent. One of the main advantages of higher-order sliding mode is it reduces chattering to a higher extent.

Consider once more the dynamical system of relative degree 1 and suppose that

$$\dot{\sigma} = h(t,x) + g(t,x)u \tag{3.1}$$

$$\phi = \int \mathbf{U}dt + \mathbf{k}\left|\sigma\right|^{2/3}\mathbf{sign}(\sigma) \tag{3.2}$$

Where $\mathbf{k}$ is positive constant

Furthermore, assume that for some positive constants

C, K_M, K_m, U_M, q

$$\left|\dot{h}\right| + U_M\left|\dot{g}\right| \le C, 0 \le K_m \le g(t,x) \le K_M, \left|\frac{h}{g}\right| < qU_M, 0 < q < 1 \tag{3.3}$$

Then the control signal becomes

$$U=-\lambda|\phi|^{\frac{1}{2}}\,sign(\phi)+u \qquad \dot{u}=\begin{cases} -u, for\ |u|>U_M \\ -\alpha sign(\phi), for\ |u|<U_M \end{cases} \quad (3.4)$$

Theorem: with $K_m\alpha > C$ and λ sufficiently large, the controller (3.3) guarantees the appearance of a 2-sliding mode $\sigma = \dot{\sigma} = 0$ in the system, which attracts the trajectories in finite time. The control u enters in finite time the segment $[-U_M, U_M]$ and stays there. It never leaves the segment, if the initial value is inside at the beginning. A sufficient (very crude!) condition for the validity of the theorem is

$$\lambda > \frac{\sqrt{\frac{2}{(K_m\alpha - C)}}(K_m\alpha + C)K_M(1+q)}{K_m^{\,2}(1-q)} \quad (3.5)$$

3.2.1.1 Design of Sliding mode control for altitude (z)

The state-space equation for altitude is as follows

$$\dot{\mathbf{x}}_5 = \mathbf{x}_6$$
$$\dot{\mathbf{x}}_6 = (\mathbf{c\varphi c\theta})\frac{\mathbf{u_1}}{\mathbf{m}} - \frac{\mathbf{k_3}}{\mathbf{m}}\mathbf{x_6} - \mathbf{g} \quad (3.6)$$

Then the linear sliding surface form $\sigma = cx_5 + x_6$ $c > 0$ is c larger then the sliding decay rate is faster. by select c be 3, then the sliding surface become

$$\sigma = 3x_5 + x_6 \quad (3.7)$$

Then computing $\dot{\sigma}$ get

$$\dot{\sigma} = 3\dot{x}_5 + \dot{x}_6 = 3x_6 + (c\varphi c\theta)\frac{u_1}{m} - \frac{k_3}{m}x_6 - g \quad (3.8)$$

from the above 3.7 we assign $h(t,x) = 3x_6 - \frac{k_3}{m}x_6 - g$

and $g(t,x) = \frac{(c\varphi c\theta)}{m}$

3.2.1.2 Design of Sliding mode control for attitude (φ, θ)

For φ

The state-space equation for pitch is as follows

$$\dot{\mathbf{x}}_7 = \mathbf{x}_8$$
$$\dot{\mathbf{x}}_8 = \mathbf{a_1u_2} + \mathbf{a_2}\bar{\Omega}_r\,\mathbf{x_{10}} + \mathbf{a_3x_{10}x_{12}} - \mathbf{k_4a_1x_8}^2 \quad (3.9)$$

Then the linear sliding surface form as $\sigma = cx_7 + x_8$ $c > 0$ it c is larger the sliding dynamics decays rate is larger. By select c be 3, then the sliding surface become

$$\sigma = 3x_7 + x_8 \quad (3.10)$$

Then computing $\dot{\sigma}$ get

$$\dot{\sigma} = 3x_8 + a_2\bar{\Omega}_r\,x_{10} + a_3x_{10}x_{12} - k_4a_1x_8^{\,2} + a_1u_2$$

(3.10)

From the above equation, we assign

$h(t,x) = 3x_8 + a_2\bar{\Omega}_r\,x_{10} + a_3x_{10}x_{12} - k_4a_1x_8^{\,2}$ and

$g(t,x) = a_1$

For θ

The state-space equation for the roll is as follows

$$\dot{\mathbf{x}}_9 = \mathbf{x_{10}}$$
$$\dot{\mathbf{x}}_{10} = \mathbf{a_4u_3} + \mathbf{a_5}\bar{\mathbf{\Omega}}_\mathbf{r}\,\mathbf{x_8} + \mathbf{a_6x_8x_{12}} - \mathbf{k_5a_4x_{10}}^{\mathbf{2}} \quad (3.11)$$

Then the linear sliding surface form as $\sigma = cx_9 + x_{10}$ $c > 0$ it c is larger the sliding dynamics decays rate is larger. By select c be 3, then the sliding surface become

$$\sigma = 3x_9 + x_{10} \quad (3.12)$$

Then computing $\dot{\sigma}$ get

$$\dot{\sigma} = 3x_{10} + a_5\bar{\Omega}_r\,x_8 + a_6x_8x_{12} - k_5a_4x_{10}^{\,2} + a_4u_3 \quad (3.13)$$

From the above equation, we assign

$h(t,x) = 3x_{10} + a_5\bar{\Omega}_r\,x_8 + a_6x_8x_{12} - k_5a_4x_{10}^{\,2}$ and

$g(t,x) = a_4$

3.2.1.3 Design of Sliding mode control for heading (Ψ)

The state-space equation for yaw is as follows

$$\dot{\mathbf{x}}_{11} = \mathbf{x_{12}}$$
$$\dot{\mathbf{x}}_{12} = \mathbf{a_8x_{10}x_8} - \mathbf{k_6a_7x_{12}}^{\mathbf{2}} + \mathbf{a_7u_4} \quad (3.14)$$

Then the linear sliding surface form as $\sigma = cx_{11} + x_{12}$ $c > 0$ it c is larger the sliding dynamics decays rate is larger. By select c be 3, then the sliding surface become

$$\sigma = 3x_{11} + x_{12} \quad (3.15)$$

Then computing $\dot{\sigma}$ we get

$$\dot{\sigma} = 3x_{12} + a_8 x_{10} x_8 - k_6 a_7 x_{12}^{\ 2} + a_7 u_4$$

(3.16)

From the above equation, we assign

$h(t,x) = 3x_{12} + a_8 x_{10} x_8 - k_6 a_7 x_{12}^{\ 2}$ and $g(t,x) = a_7$

3.4 Calculated Controller parameters for regulation

The controller parameters listed below in Table I are calculated based on the above theorem.

TABLE I. Regulation problem controller parameters for sliding mode control

Controlled variables	**Calculated Values**	
	λ for Super-twisting SMC	***α for Super-twisting SMC***
Z(altitude)	60	1
Pitch(phi)	15	5
Roll (theta)	15	5
Yaw (psi)	5	1

4. Simulation results and Analysis

4.1 Parameters used for simulation

TABLE II. Physical parameters for the quadrotor [11]

Parameters	**Calculated Parameter**
	Values and Unit
Arm Length(l)	0.5m
Total mass	0.5 kg
Quadrotor mass moment of inertia (I)	**diag** (0.005,0.005,0.01) kgm^2
Motor inertia (Jr)	$2.8385*10^{-5}$ N.m/rad/s^2
Coefficient of Lift (b)	$2.9*10^{-5}$
Coefficient of Drag (d)	$3*10^{-7}$
Aerodynamic friction Coefficients ($K_{1,2,3}$)	0.3729
Translational drag Coefficients ($K_{4,5,6}$)	$5.56*10^{-4}$
Gravitational acceleration(g)	9.81 m/s^2

4.2 Initial conditions

$$\begin{cases} z(0) = 6m \\ \dot{z}(0) = 1m/s \\ \varphi(0) = 0.174rad \\ \dot{\varphi}(0) = 1.74*10^{-3} rad/s \\ \theta(0) = 0.174rad \\ \dot{\theta}(0) = 1.74*10^{-3} rad/s \\ \psi(0) = 0.174rad \\ \dot{\psi}(0) = 1.74*10^{-3} rad/s \end{cases} \quad (3.17)$$

4.3 Simulation graphs and Analysis

For simulation purpose, the parameters listed in Table II are used.

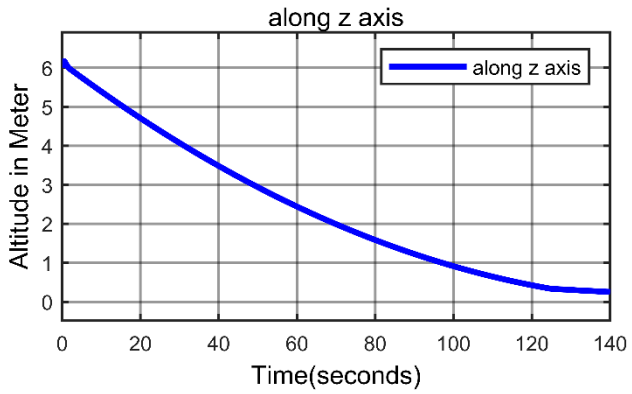

Figure 2 Altitude regulation controller performance using second-order SMC

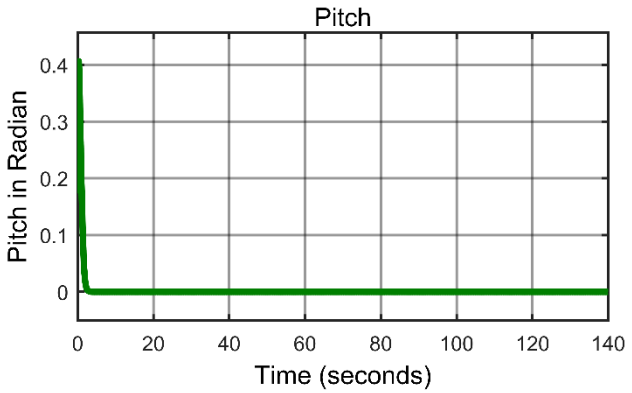

Figure 3 Pitch regulation controller performance using second-order SMC

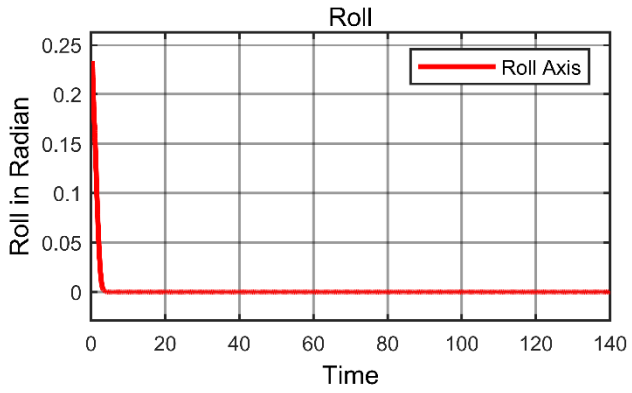

Figure 4, Roll regulation controller performance using second-order SMC

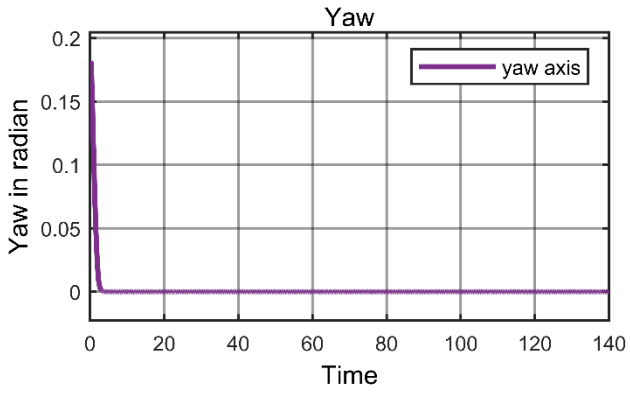

Figure 5 Yaw (heading) regulation controller performance using second-order SMC

The overall results are shown in Fig. 2, Fig. 3, Fig. 4, and Fig. 5, respectively.Fig.2 demonstrates the regulation performance of altitude, which is shown that the response of the quadrotor can regulate to zero in a very small finite time. Fig. 3, Fig. 4, and Fig. 5 show the regulation performances of three Euler angles, i.e., pitch, roll, and yaw, respectively. It shows that the quadrotor regulates to zero for three Euler angles as closely as possible with minimum error.

It can be seen from the above simulation results that the proposed third-order sliding mode control is effective and accurate.

5. Control Signal for Regulation

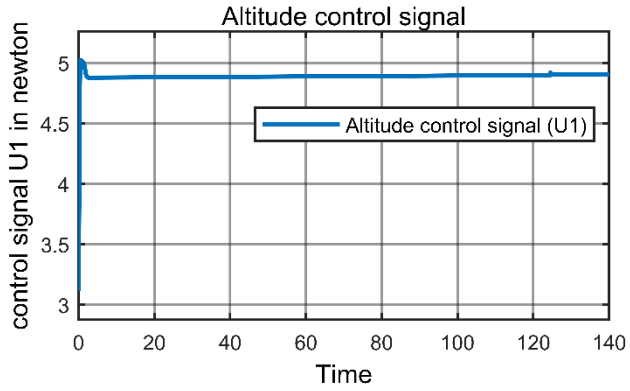

Figure 6 Altitude control signal of second-order SMC for regulation

In Fig. 6, the result shows the altitude control signal of the controller. The control signal is in the practical region. The motors can generate this amount of thrust force with 3000 rpm speed. With 3000-rpm speed, the motors can generate 6-newton force.

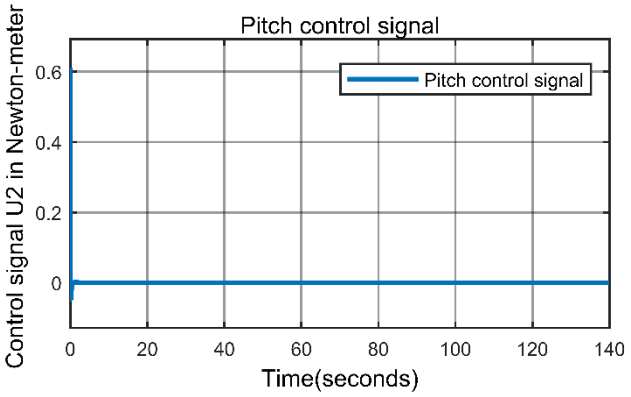

Figure 7 Pitch control signal of second-order SMC for regulation

In Fig. 7, the result shows the pitch control signal of the controller. The control signal is in the practical region. one motor can produce 1.1 newtons at 2500 rpm. Making one motor stationary and the other one rotate at 2500 rpm can get a 0.55-newton meter torque. From the figure, the maximum bound on the pitch control signal is 0.425-newton meter, which is less than 0.55-newton meter.

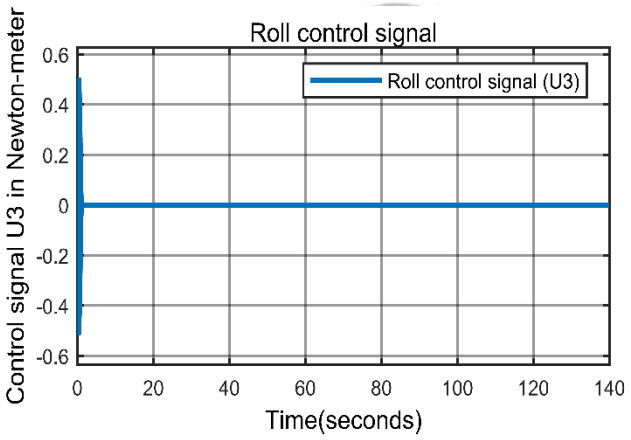

Figure 8 roll control signal of second-order SMC for regulation

In Fig. 8, the result shows the roll control signal of the controller. The control signal is in the practical region. one motor can produce 1.1 newtons at 2500 rpm. Making one motor stationary and the other one rotate at 2500 rpm can get a 0.55-newton meter torque. From the figure, the maximum bound on the roll control signal is 0.5-newton meter, which is less than 0.55-newton meter.

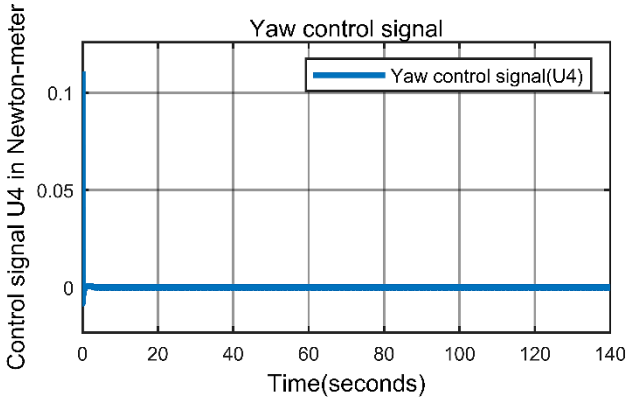

Figure 9, Yaw control signal second-order SMC for regulation

In Fig. 9, the result shows the yaw control signal of the controller. The control signal is in the practical region. One motor can produce 1.1 newtons at 2500 rpm. Making one motor stationary and the other one rotate at 2500 rpm can get a 0.55-newton meter torque. From the figure, the maximum bound on the yaw control signal is 0.05-newton meter, which is less than 0.55-newton meter.

6. Simulation of the controlled variable under external disturbance

In Table III below, there are random disturbance ranges for the four controlled variables. These parameters are used for simulation purposes.

TABLE III. Range of external disturbance parameters for simulation purposes.

Dynamics/state	Random disturbance range
Z (altitude)	-2 to 2 Newton
Pitch (phi-attitude)	-0.1 to 0.1 Newton meter
Roll (theta-attitude)	-0.6 to 0.6 Newton meter
Yaw (psi-heading)	-0.5 to 0.5 Newton meter

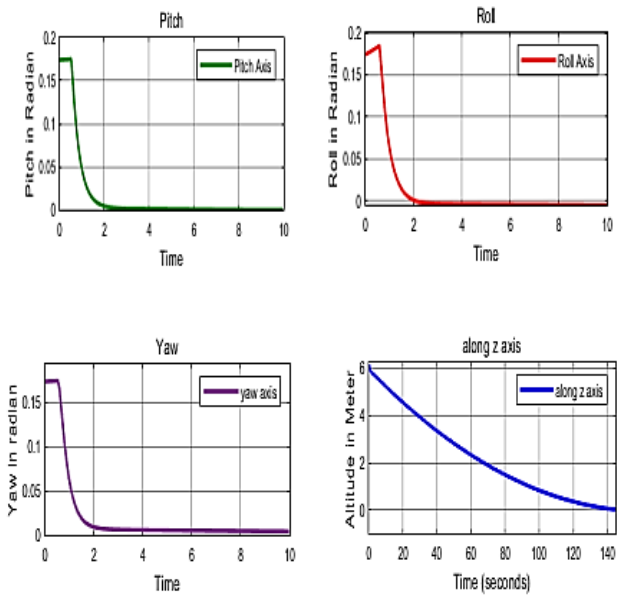

Figure 10 pitch, roll, altitude, and yaw simulation under the influence of external disturbance

In Fig. 10, the result shows the performance of the four third-order SMC controllers (altitude, pitch, roll, and yaw) under the influence of random disturbance. As we see from the graphs, the controllers regulate the quadrotor physical system under the influence of external random disturbance. The controllers are robust.

Conclusion

In this paper, the nonlinear dynamic model of the quadrotor is derived using the Lagrange formalism. The model contains two parts, namely, translational and rotational dynamics (Euler-angle dynamics). The nonlinear model includes the gyroscopic moments induced due to the rotational motion of the quadrotor body & propellers mounted on the rotor . Besides, the aerodynamic friction moment & force are considered in the modeling. After the derivation of the dynamic model, a nonlinear control strategy (Third-order SMC) based on the supertwisting algorithm is designed.

To verify the performance and efficiency of the controller, a simulation is done via Matlab/Simulink. The third-order SMC is designed for four output-controlled variables separately. The controlled variables are altitude, pitch, roll, and yaw. The third-order SMC is implemented on the physical system for the regulation problem. The controller is excellent; it can regulate the physical system with fast & smooth response and good stability. The control effort used by the controller to regulate the system is so small and within a practical limit. Finally, the controller performance was tested by adding random disturbance to the system. The controller achieves excellent performance in the presence of external disturbance. Overall, the higher-order SMC controller designed for the quadrotor system is robust and has an excellent performance.

References

[1] Vachtsevanos, Kimon P. Valavanis, George J., Handbook UAV, New York, London: Springer, 2015.
[2] R. Jategaonkar, Flight vehicle system identification a time-domain methodology, Reston, Virginia: American Institute of Aeronautics and Astronautics Inc, 2015.
[3] Q. Quan, Introduction to Multicopter Design and Design, Beijing, China: Springer, 2017.
[4] D. Norris, Build Your Quadcopter, New York, Chicago: McGraw-Hill Education, 2014.
[5] P. Johan From, J. Tommy Gravdahl, K. Ytterstad Pettersen, Vehicle Manipulator System, Verlag, London: Springler, 2014.
[6] D. Lee, H. Jin Kim, and S. Sastry, "Feedback linearization vs. adaptive sliding mode control for a quadrotor helicopter," *International Journal of Control Automation and Systems*, vol. 3, no. 7, pp. pp. 419-428, 2009.
[7] S. Bouabdallah, A. Noth, and R. Siegwart, "PID vs LQ control techniques applied to an indoor micro quadrotor," *in International Conference on Intelligent Robots and Systems*, 2004.
[8] S. Bouabdallah, "Design and Control of Quadrotors with Application to Autonomous Flying," *OAI, MSc thesis Zurich*, vol. 10, no. 5775, 2007.
[9] A. REZOUG, M. HAMERLAIN, Z. ACHOUR, and M. TADJINE, "Applied of an Adaptive Higher Order Sliding Mode Controller to Quadrotor Trajectory Tracking," in *IEEE International Conference on Control System, Computing and Engineering*, Penang, Malaysia, November 2015.
[10] O. Gherouat, D. Matouk, A. Hassam, and F. Abdessemed, "Modeling and Sliding Mode Control of a Quadrotor Unmanned Aerial Vehicle," *J. Automation and Systems Engineering*, vol. 10, no. 3, pp. 150-157, 2016.
[11]Abraham Villanueva, B. Castillo-Toledo, and Eduardo Bayro-Corrochano, "Multi-mode Flight Sliding Mode Control System for a Quadrotor," in *2015 International Conference on Unmanned Aircraft Systems (ICUAS)*, Denver, Colorado, USA, June 2015.
[12] Yi Kui, Gu Feng, Yang Liying, He Yuqing, Han Jianda, "Sliding Mode Control for a Quadrotor Slung Load System," in *Proceedings of the 36th Chinese Control Conference*, Dalian, China, July 26-28, 2017.
[13] S. Bouabdallah, A. Noth and R. Siegwart, PID vs. LQ Control Techniques Applied to an Indoor Micro Quadrotor, Proceedings of the 2004 IEEE/RSJ International Conference on Intelligent Robots and Systems, pp. 2451–2456, Sendai, Japan, October 2004.
[14] S. Khatoon, D. Gupta, and L.K. Das, PID, and LQR control for a Quadrotor: Modeling and simulation, *Proceedings of the 2014* International Conference *on Advances in Computing*, Communications, and Informatics, pp. 796–802, New Delhi, September 2014.
[15] V.G. Adr, A.M. Stoica and J.F. Whidborne, Sliding mode control of a4Y octocopter, *UPB Scientific Bulletin, Series D: Mechanical EngineeringJournal*, vol. 74, no. 4, pp. 37-52, 2012.
[16] E-H. Zheng, J-J. Xiong and J-L. Luo, Second-Order Sliding mode control for a Quadrotor UAV, *ISA Transactions*, vol. 53, no. 4, pp. 1350–1356, 2014.
[17] L. Besnard, Y.B. Shtessel and B. Landrum, Quadrotor Vehicle Control via Sliding Mode Controller Driven by Sliding Mode Disturbance Observer, *Journal of the Franklin Institute*, vol. 349, pp. 658–684, 2012.

[18] J-J.E. Slotine and W. Li, *Applied nonlinear control*, Prentice-Hall, Englewood Cliffs, New Jersey, 1991.
[19] G.V. Raffo, M.G. Ortega, and F.R. Rubio, An Integral Predictive/Nonlinear *H1* Control Structure for a Quadrotor Helicopter, *Automatica*, vol. 46, no.1, pp. 29–39, 2010.
[20] S. Islam, J. Dias, and L.D. Seneviratne, Adaptive tracking control for Quadrotor unmanned flying vehicle, *Proceedings of the 2014 IEEE/ASME International Conference on Advanced Intelligent Mechatronics (AIM)*, pp. 441–445, Besanon, France, July 2014.

APPENDICES

Proof of theorem

Computing with $|u| > U_M$ yields $\dot{u} = \frac{-1}{2}\lambda\dot{\sigma}|\sigma|^{\frac{-1}{2}} - u$. It follows from Eqs. (3.2), (3.3) in the text that that $\dot{\sigma}u > 0$ with $|u| > U_M$ and thus, $u\dot{u} < 0$, and u moves

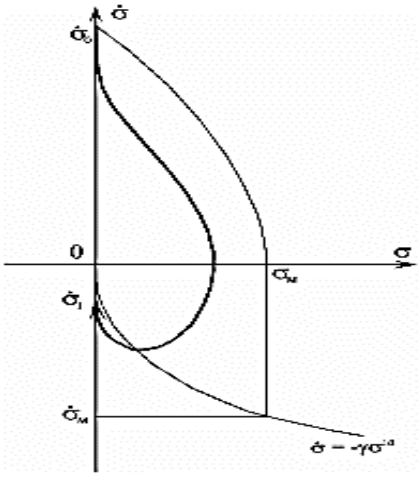

Figure 1 A majoring curve for the super twisting controller

towards the segment $|u| \le U_M$. Therefore $|u| \le U_M$ is established in finite time, for $|\dot{u}| > U_M$ when $|u| > U_M$. Note that a 1-sliding mode with $u = -U_m sign(\sigma)$ could exist during time intervals of constant $sign(\sigma)$ .the following equation is satisfied with $|u| < U_M$, $\sigma \neq 0$:

$$\ddot{\sigma} = \dot{h} + \dot{g}u - g0.5\lambda\frac{\dot{\sigma}}{|\sigma|^{1/2}} - g\alpha sign(\sigma)$$

The trivial identity $\frac{d}{dt}|\sigma| = \dot{\sigma}\,sign(\sigma)$ is used here. Note that once more, the values taken on sets of measure 0 are not accounted for; thus, the differentiation is performed with $sign(\sigma) = const$. The latter equation may be rewritten as

$$\ddot{\sigma} \in [-C, C] - [K_m, K_M]\left(\frac{1}{2}\lambda\frac{|\dot{\sigma}|}{|\sigma|^{1/2}} + \alpha sign(\sigma)\right)$$

This inclusion does not 'remember' anything about the original system. With $\sigma > 0$, $\dot{\sigma} > 0$, the real trajectory is confined by the axes $\sigma = 0$ $\dot{\sigma} > 0$ and the trajectory of the equation $\ddot{\sigma} = -(K_m\alpha - C)$. Let σ_M be the intersection of this curve with the axis $\dot{\sigma} = 0$. Obviously, $2(K_m\alpha - C)\sigma_M = \dot{\sigma}_0^2$ (Fig.1). It is easy to see from Fig. 1 that

$$\sigma > 0, \dot{\sigma} > 0, \frac{1}{2}\lambda\frac{|\dot{\sigma}|}{|\sigma|^{1/2}} > \frac{C}{K_m} + \alpha \Rightarrow \ddot{\sigma} > 0$$

Thus, the majoring curve $\sigma > 0$ is constructed from the following curves (3):

$$\dot{\sigma}^2 = 2(K_m\alpha - C)(\sigma_M - \sigma) \text{ with } \dot{\sigma} > 0,$$

$$2(K_m\alpha - C)\sigma_M = \dot{\sigma}_0^2$$

$$\sigma = \sigma_M \text{ with } 0 \ge \dot{\sigma} \ge \frac{2}{\lambda}\left(\frac{C}{K_m} + \alpha\right)\sigma^{1/2}$$

$$\dot{\sigma} = \dot{\sigma}_M = -\frac{2}{\lambda}\left(\frac{C}{K_m} + \alpha\right)\sigma_M^{1/2} \text{ with } 0 \le \sigma \le \sigma_M$$

The condition $|\dot{\sigma}_M / \dot{\sigma}_0| < 1$ is sufficient for the algorithm while $|u| < U_M$. That condition is rewritten as

$$\frac{2(K_m\alpha + C)^2}{\lambda^2 K_m^{\,2}(K_m\alpha - C)} < 1$$

Unfortunately, the latter inequality is still not sufficient, for this consideration does not include the possible 1-sliding mode keeping $u = \pm U_M$.

It is easy to see that such a mode is not possible $\sigma\dot{\sigma} > 0$.

Indeed, in that case, $u\dot{\sigma}$ stays negative and does not allow

any sign switching of $u - U_M$ .on the other hand, from Eqs. (3.2), (3.3) and $|u| \le U_M$, in such a sliding mode

$$K_m(1-q)U_M \le \left|\dot{\sigma}\right| = g\left|\frac{h}{g} + u\right| \le K_M\,(1+q)U_M$$

Thus, $\dot{\sigma}_0 \le K_M\,(1+q)U_M$, and the condition

$$\left|\frac{\dot{\sigma}_M}{\dot{\sigma}_0}\right| < \frac{K_m(1-q)U_M}{K_M(1+q)U_M} = \frac{K_m(1-q)}{K_M(1+q)}$$

Is sufficient to avoid keeping $u = \pm U_M$ in sliding mode. The resulting condition above coincides with eq. (3.5) in text.

This completes the proof of the theorem.